Injectable Dual-Gelling Cell-Laden Composite Hydrogels for Bone Tissue Engineering

T.N. Vo[a], **S.R. Shah**[a], **S. Lu**[a], **A.M. Tatara**[a], **E.J. Lee**[a], **T.T. Roh**[a], **Y. Tabata**[b], and **A.G. Mikos**[a,c,*]

[a]Department of Bioengineering, Rice University, P.O. Box 1892, MS 142, Houston, Texas, 77251-1892, USA

[b]Department of Biomaterials, Institute for Frontier Medical Sciences, Kyoto University, Kyoto, Japan

[c]Department of Chemical and Biomolecular Engineering, Rice University, P.O. Box 1892, MS 362, Houston, Texas, 77251-1892, USA

Abstract

The present work investigated the osteogenic potential of injectable, dual thermally and chemically gelable composite hydrogels for mesenchymal stem cell (MSC) delivery *in vitro* and *in vivo*. Composite hydrogels comprising copolymer macromers of *N*-isopropylacrylamide were fabricated through the incorporation of gelatin microparticles (GMPs) as enzymatically digestible porogens and sites for cellular attachment. High and low polymer content hydrogels with and without GMP loading were shown to successfully encapsulate viable MSCs and maintain their survival over 28 days *in vitro*. GMP incorporation was also shown to modulate alkaline phosphatase production, but enhanced hydrogel mineralization along with higher polymer content even in the absence of cells. Moreover, the regenerative capacity of 2 mm thick hydrogels with GMPs only, MSCs only, or GMPs and MSCs was evaluated *in vivo* in an 8 mm rat critical size cranial defect for 4 and 12 weeks. GMP incorporation led to enhanced bony bridging and mineralization within the defect at each timepoint, and direct bone-implant contact as determined by microcomputed tomography and histological scoring, respectively. Encapsulation of both GMPs and MSCs enabled hydrogel degradation leading to significant tissue infiltration and osteoid formation. The results suggest that these injectable, dual-gelling cell-laden composite hydrogels can facilitate bone ingrowth and integration, warranting further investigation for bone tissue engineering.

*Corresponding author: Dr. Antonios G. Mikos, Department of Bioengineering, Rice University, P.O. Box 1892, MS 142, Houston, Texas, 77251-1892, USA., Tel.: +001-713-348-5355, Fax: +001-713-348-4244, mikos@rice.edu.

Keywords

gelatin microparticles; *N*-isopropylacrylamide; critical size cranial defect; mesenchymal stem cells; mineralization

1. Introduction

The craniofacial bone provides the natural contouring of the face as well as mechanical support of the overlying tissues. Current treatments for craniofacial injury resulting from trauma, disease, or congenital defects rely on the use of bone grafts taken from the patient or a donor that require extensive reshaping and multiple invasive surgeries. Tissue engineering provides a strategy by which combinations of biomaterial scaffolds, cells and/or growth factors can be designed for minimally invasive aesthetic and functional reconstruction [1, 2]. Thus, injectable, *in situ* forming hydrogels are attractive candidates for craniofacial bone tissue engineering applications. These materials can be prepared as aqueous solutions at room temperature, allowing easy mixing of cells or growth factors, and administered minimally invasively via injection whereby the material can conform to and support the defect during regeneration.

We previously reported on the development and characterization of an injectable, *in situ* forming hydrogel system based on *N*-isopropylacrylamide (NiPAAm) [3, 4]. By copolymerizing NiPAAm with epoxy pendant rings and lactone moieties to form a thermogelling macromer (TGM), an injectable dual-gelling hydrogel system was created that could both thermally and chemically gel with a diamine-functionalized polyamidoamine (PAMAM) crosslinker, form *in situ*, and hydrolytically degrade over time. Previous work has demonstrated the hydrogel's rapid and dual gelation without syneresis, tunable physiochemical properties, biocompatibility *in vivo*, and hydrophobicity-dependent mineralization [3, 4].

The objective of this work was to evaluate the osteogenic potential and regenerative capacity of an injectable dual-gelling hydrogel system for stem cell delivery *in vitro* and *in vivo*. Mesenchymal stem cells (MSCs) were chosen as the cell source due to their established multipotent differentiation potential, particularly down the osteogenic lineage, availability and ease of sourcing, and proliferative capacity *in vitro* [5]. Additionally, MSCs interact through paracrine signaling processes to modulate the behavior of host cells and the inflammatory response that may promote a favorable regenerative outcome [5]. In order to provide sites for cellular attachment within the synthetic hydrogel and enhance hydrolysis-dependent degradation, gelatin microparticles (GMPs) were added as an enzymatically digestible porogen [6]. We hypothesized that viable MSC-laden hydrogels could be formed and that the hydrogels could modulate encapsulated cell viability, osteogenic differentiation, and hydrogel mineralization *in vitro* through TGM content and incorporation of GMPs. Additionally, when implanted in an 8 mm rat critical size cranial defect, the composite hydrogel constructs with both GMPs and MSCs were hypothesized to enhance bone regeneration, as assessed through microcomputed tomography (microCT) of bony bridging and bone volume, and improve tissue integration and infiltration, as evaluated through histological scoring, compared to hydrogels with either GMPs or MSCs alone.

2. Materials and Methods

2.1 Materials

NiPAAm, dimethyl-γ-butyrolactone acrylate (DBA), glycidyl methacrylate (GMA), acrylic acid (AA), 2,2'-azobis(2-methylpropionitrile) (azobisisobutyronitrile, AIBN), *N,N'*-methylenebisacrylamide (MBA), piperazine (PiP), glycine, and glutaraldehyde were purchased from Sigma Aldrich (Sigma, St. Louis, MO) and used as received. Anhydrous 1,4-dioxane, diethyl ether, and acetone in analytical grade; and water, acetonitrile, chloroform, and methanol in HPLC-grade were purchased from VWR (Radnor, PA) and used as received. PBS (powder, pH 7.4) was obtained from Gibco Life, Grand Island, NY. Ultrapure water was obtained from a Millipore Super-Q water system (Millipore, Billerica, MA). Acidic gelatin (IEP=5.0) was obtained from Nitta Gelatin (Osaka, Japan). Complete osteogenic medium (COM) was made from minimal essential medium α modification (αMEM) (Gibco Life, Grand Island, NY) supplemented with 10% fetal bovine serum (FBS) (Cambrex BioScience, Walkersville, MD), 10^{-8} M dexamethasone, 10 mM β-glycerol 2-phosphate, 50 mg/L ascorbic acid, and 10 mL/L antibiotic-antimycotic solution (Gibco, Life, Grand Island, NY). Live/Dead viability/cytotoxicity kit was purchased from Molecular Probes (Eugene, OR). The calcium assay was purchased from Genzyme Diagnostics (Cambridge, MA).

2.2 TGM synthesis and characterization

Synthesis of P(NiPAAm-*co*-GMA-*co*-DBA-*co*-AA) TGMs were performed according to published protocols [4]. Briefly, 10 g of NiPAAm, GMA, DBA and AA were dissolved in 200 mL of anhydrous 1,4-dioxane under nitrogen at 65°C. AIBN pre-dissolved in the solvent was added at 0.7% of total mol content of the comonomers to thermally initiate free radical polymerization, and the reaction mixture was stirred for 16 h. After solvent removal by rotary evaporation, the material was re-dissolved in pure acetone and purified twice via dropwise precipitation in at least 10X excess diethyl ether. The recovered polymer was air-dried overnight and transferred to a vacuum oven for several days prior to elemental analysis. The chemical composition of the TGMs was determined by proton nuclear magnetic resonance spectroscopy (^{1}H NMR, Bruker, Switzerland) in D_2O at a concentration of 20 mg/mL that contained 0.75 wt% 3- (trimethylsilyl)propionic-2,2,3,3-d4 acid sodium salt as an internal shift reference (Sigma-Aldrich, St. Louis, MO). Acid titration was performed in conjunction with ^{1}H NMR to determine the AA content of the TGMs before hydrolysis. Aqueous gel permeation chromatography using a Waters Alliance HPLC system (Milford, MA) and differential refractometer (Waters, model 410) equipped with a series of analytical columns (Waters Styragel guard column 20 mm, 4.6 x 30 mm; Waters Ultrahydrogel column 1000, 7.8 x 300 mm) was used to determine the molecular weight distributions of the synthesized TGM. The weight average molecular weight (M_w), number average molecular weight (M_n), and polydispersity index (PDI = M_w/M_n) of the hydrolyzed polymer were determined by comparison to commercially available narrowly dispersed molecular weight poly(ethylene glycol) standards (Waters, Mississauga, ON). For this study, P(NiPAAm$_{85.6}$-*co*-GMA$_{6.0}$-*co*-DBA$_{5.5}$-*co*-AA$_{2.9}$) with a M_n = 36.4 kDa and PDI of 3.8 demonstrating 30% hydrolysis-dependent degradation over 10 weeks was used.

2.3 PAMAM synthesis and characterization

PAMAM was synthesized by the polyaddition of PiP and MBA at a stoichiometric molar ratio of [MBA]/[PiP] = 0.75 or 0.83 following previously reported protocols [7]. Molecular weight distributions of the synthesized PAMAM crosslinkers were analyzed using time-of-flight mass spectroscopy with positive-mode electrospray ionization on a Bruker microTOF ESI spectrometer (Bruker Daltonics, Billerica, MA) equipped with a 1200 series HPLC (Agilent Technologies, Santa Clara, CA) to deliver the mobile phase (50:50 HPLC-grade water and methanol). After data acquisition, all peaks (including degradation and secondary reaction products) were identified using microTOF Control software (Bruker). The peaks were corrected for charge state (generally with H^+ or Na^+ and rarely K^+ ions), and quantified for calculation of M_n, M_w, and PDI. PAMAM with M_n = 1440 or 2600 Da and PDI = 1.38 or 1.31, respectively were used for composite hydrogel characterization. The shorter molecular weight PAMAM crosslinker (P-1440) at a 1:1 amine epoxy mol ratio was chosen for the remaining MSC encapsulation studies.

2.4 GMP synthesis

GMPs with 50–100 μm diameter were synthesized through a water-in-oil emulsion followed by crosslinking in 10 mM glutaraldehyde solution and quenching with glycine as previously described [8]. Following fabrication, the GMPs were vacuum filtered, flash frozen in liquid nitrogen, lyophilized, and sieved.

2.5 Composite fabrication and characterization

Composite hydrogels were fabricated by combining the TGM and PAMAM crosslinker that were prepared at twice the desired concentrations in sterile phosphate buffered saline (PBS) pH 7.4 at 4°C until dissolved. GMPs were partially swelled in PBS pH 7.4 for 15 h at 4°C prior to hydrogel encapsulation as performed previously [8] and transferred to the polymer mixture. The resulting solution was manually mixed in the glass vial and transferred to 6 mm diameter x 3 mm height cylindrical Teflon molds at 37°C, and allowed to gel for 24 h.

Composite hydrogel swelling behavior was assessed with formulations of varying TGM wt % and PAMAM molecular weight. Following fabrication, the hydrogels were weighed on a balance (n=6) and placed in excess PBS for 24 h at 37°C. Hydrogels were then weighed after swelling, frozen at −80°C, lyophilized and reweighed when dry. The initial ($q_{(i)}$) and equilibrium ($q_{(e)}$) hydrogel swelling ratio were calculated as the difference between the swollen and dry mass divided by the dry mass [9].

The effect of varying TGM wt%, GMP loading, and culture condition (n = 6 per group) on hydrogel mechanical properties after 28 days was investigated. Mechanical testing on a TA Instruments Thermomechanical Analyzer 2940 (TA Instruments, Newcastle, DE) equipped with a wide compression probe (diameter of 6 mm) was performed to assess the unconfined compressive Young's modulus of the hydrogels. Samples were first placed onto the prewarmed stage, and sample height was measured by the probe. The stage was then re-equilibrated to 37°C and the sample was compressed at a rate of 0.001 N/min to 0.05 N. The unconfined Young's modulus was determined to be the initial slope of the engineering strain versus engineering stress curve.

2.6 MSC harvest and culture

MSCs were harvested from rat femora and tibiae of 6–8 week old Fisher 344 rats (Charles River Laboratories, Wilmington, MA) in accordance to approved protocols by the Rice Institutional Animal Care and Use Committee as previously described [10]. The MSCs were plated in 75 cm^2 tissue culture flasks at 37°C under humidified, 5% CO_2 atmosphere and cultured in osteogenic media without dexamethasone, which was replaced every 2–3 days.

2.7 MSC encapsulation and in vitro culture

For the *in vitro* and *in vivo* MSC encapsulation studies, TGM and PAMAM olymers were UV sterilized for 3 h, GMPs were EO sterilized for 12 h, and all polymers were dissolved in PBS pH 7.4 as described above. After 6 days of culture, the MSCs were passaged and added to the polymer solutions at a final concentration of 15 million cells/mL hydrogel. The solutions were manually mixed, pipetted into 8 mm x 2 mm autoclaved Teflon molds on a heat block, and allowed to crosslink at 37°C in an incubator for 2.5 h before *in vitro* culture or 24 h before *in vivo* implantation. The formulations selected for *in vitro* investigation are listed in Table 1. The hydrogels and their acellular controls were placed in 2.5 mL media in 12-well tissue culture plates and cultured for 0, 7, 14, 21, and 28 days in complete osteogenic media containing 10^{-8} M dexamethasone, a potent stimulator of osteogenesis [11]. At each timepoint, the hydrogels were soaked in PBS for 30 min, sliced in half, weighed, and processed for Live/Dead confocal imaging (n = 2 halves); DNA Picogreen assay, alkaline phosphatase (ALP) activity, and calcium biochemical assay (n = 4 halves each); and histological staining (n = 2 halves).

2.8 Live/Dead Confocal Microscopy

The samples designated for Live/Dead confocal microscopy were cut into ~0.5 mm cross sectional slices with a hand-held razor blade and incubated for 30 min with calcein AM (2 μM) and ethidium homodimer-1 (4 μM) in accordance with the Live/Dead viability/cytotoxicity kit instructions. The slices were then analyzed using a confocal microscope (LSM 510 META, Carl Zeiss, Germany) using a 10x objective. Argon and helium–neon lasers were used for excitation at 488 and 543 nm, respectively, and emission filters at 505–526 and 612–644 nm, respectively, were employed.

2.9 Biochemical Assays

Hydrogel halves for biochemical assays were stored in 500 μL of ultrapure water and stored at -20°C. Prior to analysis, samples were manually homogenized, passed through three freeze-thaw cycles, and probe sonicated for 8 s. Detailed protocols for biochemical assays are described elsewhere [12]. Double-stranded DNA correlating with cellularity was evaluated using DNA Picogreen assay (Invitrogen, Eugene, OR) in accordance to the manufacturer's protocol. Activity of ALP, an osteogenic marker produced by differentiating MSCs, was assessed with colorimetric assay using phosphatase substrate capsules in alkaline buffer solution against p-nitrophenol standards. To quantify the calcium content, sample aliquots were digested overnight in equal parts 1N acetic acid to form a final 0.5N acetic acid solution and then evaluated according to the manufacturer's instructions. All data were normalized to the hydrogel wet mass.

2.10 Cryosectioning and histological staining

Hydrogels (n = 2 halves) were processed at each timepoint for hematoxylin & eosin (H&E) and von Kossa histological staining as previously described [10, 13]. Hydrogels were fixed at 37 °C for 24 h in 10% buffe red formalin, dehydrated for 24 h in 70% ethanol, and stored in Histo-prep for another 24 h prior to freezing at −20 °C and cryosectioning into 10 μm slices. H&E staining for cellular distribution and extracellular matrix deposition was performed using Mayer hematoxylin counterstained with eosin-Y (Sigma). Von Kossa, a commonly used stain for phosphate deposits in bone tissue engineering studies, was performed using a 2% silver nitrate solution incubated under UV for 20 min and unreacted silver nitrate was removed using 5% sodium thiosulfate. Sections were imaged with a light microscope (Eclipse E600, Nikon).

2.11 Animal surgery, post-operative monitoring and implant harvest

This work was done in accordance with protocols approved by the Rice University Institutional Animal Care and Use Committee. The hydrogels listed in Table 2 were aseptically fabricated in 8 mm x 2 mm molds as described above and implanted within an 8 mm rat cranial defect for evaluation at 4 and 12 weeks. The hydrogels were pre-formed to ensure consistent size and homogenous fabrication allowing for accurate assessment post-implantation, especially in regards to hydrogel fragmentation due to GMP incorporation. All hydrogel groups were statistically randomized to minimize operative- or animal-related error. Using 11–12 week Fischer 344 rats weighing 176–200g (Harlan, Indianapolis, IN), an 8 mm craniotomy was performed under general anesthesia as previously described [14]. The calvarial disk was removed, the hydrogel was implanted, and the periosteum and skin were each separately closed. The rats were given a single intraperitoneal injection of saline (1 mL/100 g/h of anesthesia) and then buprenorphine (0.05 mg/kg) (Patterson Veterinary, Devens, MA) at 12, 24, and 36 h after surgery as analgesia, and were monitored post-operatively for the duration of the study. At the designated timepoints, the animals were euthanized, and the implants and surrounding tissue were harvested, fixed, and processed for microcomputed tomography and histology analysis as previously described [3, 14].

2.12 Microcomputed tomography (microCT) analysis

MicroCT analysis with a Skyscan 1172 High-Resolution Micro-CT (Aartselaar, Belgium) with 10 μm resolution, 0.5 mm aluminum filter, and voltage of 100 kV and current of 100 μA was used to evaluate bone volume and bony bridging across the defect. Volumetric reconstruction and analysis was conducted using Nrecon and CT-analyzer software provided by Skyscan. The percent of bone formation, including hydrogel mineralization, within the defect was determined by centering a cylindrical volume of interest (VOI) of 8 mm in diameter and 2 mm in height at the bottom of the defect. Data are reported as the % binarized object volume measured within this VOI within thresholding gray values (70–255) with the CT-analysis software [15]. The extent of bony bridging and union within the defect were scored according to the grading scale in Supplementary Figure 1 using microCT generated maximum intensity projections of the samples. 3D models of each sample were also generated to visualize the distribution of mineral deposits within the hydrogel implants.

2.13 Histological Scoring

After microCT scanning, the samples were sent to the MD Anderson Cancer Center Bone Histomorphometry Core Laboratory (Houston, TX) for dehydration and embedding in poly(methyl methacrylate). 5 μm coronal cross-sections were taken from the center of the defect of each sample and staining was performed with von Kossa, H&E, and Goldner's trichrome. The three histological sections were evaluated via light microscopy and scored using histological scoring analysis with three blinded reviewers. The histological evaluation was performed along random implant-tissue interfaces within central coronal cross-sections to assess: (1) tissue response at the bone-hydrogel interface [16], (2) fibrous capsule thickness and quality on the dural and periosteal sides of the implant [17], and (3) extent of bony bridging across the defect following the rubrics outlined in Supplementary Figure 1. Additionally, the degree of hydrogel fragmentation due to tissue infiltration was scored according to previously published literature [13, 18].

2.14 Statistics

The data are presented as mean + standard deviation in triplicate, unless otherwise stated. Composite characterization data and biochemical assays were analyzed using a Tukey's post-hoc test. Main effects and interaction analysis of hydrogel swelling were performed with JMP v.11 statistics software (SAS Institute, Cary, NC). The microCT and histological scoring data were analyzed via one-way analysis of variance followed by the Kruskal-Wallis test ($p<0.05$) for n = 7–8 samples. The microCT bone volume data were for n = 7–8 samples.

3. Results

3.1 Composite hydrogel fabrication and characterization

Composites hydrogels were successfully created by mixing together TGMs, PAMAMs, and pre-swollen GMPs. Incorporation of GMPs did not hinder the secondary chemical crosslinking of TGMs and PAMAMs, and a stable hydrogel was formed within the previously established period of 2.5 h [4]. A partial factorial design study examining the effect of TGM wt% and PAMAM M_n demonstrated that GMP loading did not significantly affect initial and equilibrium swelling compared to non-gelatin containing hydrogels (Supplementary Figure 2A), and also did not affect the compressive properties even after culture in complete osteogenic media containing serum (Supplementary Figure 2B).

3.2 In vitro MSC encapsulation

10 and 20 wt% hydrogels with and without GMPs were able to successfully encapsulate primary rat MSCs to form hydrogel-cell constructs. Encapsulating cells in serum-containing media did not significantly affect hydrogel gelation, and after 2.5 h, a stable hydrogel was formed. Figure 1A shows representative cross sections of 10 wt% hydrogels with and without gelatin microparticles using Live/Dead confocal microscopy after culture for 0, 7, 14, 21, and 28 days. The 20 wt% hydrogels performed similarly and confocal images can be seen in Supplementary Figure 3. The 0 d images showed that viable MSCs could be encapsulated (as shown by the green stain for live cells) without significant cell death (as shown by the red stain for dead cells) and homogenously distributed throughout the

hydrogel, which was confirmed with H&E staining (data not shown). Confocal imaging at the other timepoints demonstrated that cell viability could be maintained throughout the hydrogels over the 28 day culture period, and was higher at the later timepoints when GMPs were incorporated.

3.3 Biochemical assays and histology

DNA Picogreen data correlating to cellularity are shown in Figure 1B. DNA content in the non-GMP-containing hydrogels significantly decreased over time; however, DNA content in the GMP-containing hydrogels was sustained over time since no significant differences were observed in the DNA levels from the 7 to 28 day timepoints, and showed significant improvements over the non-GMP-containing hydrogel counterparts at the later timepoints.

ALP is an enzyme produced by osteogenically differentiating MSCs. Figure 2 shows the ALP activity of the hydrogel-MSC constructs normalized to the DNA content over time. Two profiles were observed depending on the incorporation of GMPs. Non-GMP-containing hydrogels showed significant increases in the ALP activity over time, peaking at 21 days, and then declining. The GMP-containing hydrogels did not show significant changes in their ALP activity, with the exception of the 10 wt% hydrogels with GMPs at two timepoints. However, when comparing across groups at the later timepoint, the ALP activity of the non-GMP-containing hydrogels was significantly higher.

Mineralization of the hydrogels was evaluated using a calcium biochemical assay, and compared to acellular controls (Figure 3B). In all groups, hydrogels demonstrated significant increases in calcium content over time, which was reflected in the darker von Kossa staining at 28 days (Figure 3A). 20 wt% hydrogels showed significantly greater calcium content than 10 wt% hydrogels. GMP-containing hydrogels also showed significantly greater calcium content than non-GMP-containing hydrogels. Except for the 20 wt% GMP-containing hydrogel with cells, all other groups demonstrated mineralization that was not significantly greater than their respective acellular control.

3.4 Animal Care

Three groups of 20 wt% hydrogels were investigated in the rat cranial defect model: hydrogels with GMPs only (Gel+GMP), hydrogels with MSCs only (Gel+MSC), and hydrogels with GMPs and MSCs (Gel+GMP+MSC). Surgery was performed on 47 rats, of which one (Gel+GMP+MSC at 4 weeks) was excluded after harvest since the hydrogel dislocated from the defect site post-operatively. All other samples were included in the microCT and histological analyses.

3.5 MicroCT analysis

MicroCT was used for nondestructive and quantitative analysis of bony bridging and bone volume, as well as visualization of mineral distribution. To evaluate bony bridging, maximum intensity projections (MIPs) of each sample were generated from the microCT datasets and scored by three blinded reviewers according to a 0–4 scale as seen in Supplementary Figure 1. Figure 4A shows representative MIPs from each group at each timepoint with their respective scores. The presence of partial bony bridging in most of the

samples is reflected in the average microCT score of 2 as seen in Figure 4B. However, only the Gel+GMP group demonstrated a significant improvement in bony bridging over the two timepoints.

MicroCT was also used to quantify the bone volume within the 8 mm x 2 mm VOI, which includes mineralization throughout the hydrogel as well as above and below the implant. Figure 4C shows the bone volume data as a % binarized object volume above a critical threshold grayscale value of 70. Similar to the microCT bony bridging results, only the Gel +GMP group demonstrated a significant improvement in bony bridging over the two timepoints.

3.6 Histological analysis

Figure 5 shows representative histological sections of the samples from each group and timepoint following H&E, von Kossa, and Goldner's trichrome staining. For all the samples, the hydrogel can be observed, although some minor artifacts due to delamination and mechanical mismatch during slice can be seen. At both the 4 and 12 week timepoints, the samples have a well defined and organized fibrous capsule surrounding much of the implant. However, there are cases among all the groups where robust bone growth is observed across the dural side of the implant that is in direct contact with the hydrogel. Additionally, instances of mineralization within the hydrogel volume and tissue infiltration can be observed in many of the samples. This is more clearly seen when juxtaposed with the gross implant images and microCT MIPs, as shown with representative samples in Figure 6. Figure 6A shows the presence of new mineral on the hydrogel implant using microCT, which can be visually observed as an opaque white mass in the translucent implant. Figure 6B shows a microCT MIP demonstrating the presence of mineralization throughout the hydrogel volume that is in direct contact with the surrounding hydrogel and osteoid when examined through high magnification von Kossa histological stains.

To quantify the regenerative capacity of the hydrogels, histological scoring according to the guides in Supplementary Figure 1 was performed to specifically assess bony bridging, tissue response at bone-implant interfaces, fibrous capsule thickness and quality, and hydrogel fragmentation. Figure 7A shows the results for scoring of bony bridging in the histological sections across the dural side of the hydrogel. The Gel+GMP hydrogels were the only group to demonstrate significant differences between the two timepoints. To assess tissue response, two independent scoring guides were used for the bone-implant interface and the fibrous capsule surrounding the rest of the implant. Figure 7B shows the combined scores for the tissue response at the left and right interfaces. The scores for each interface are shown in Supplementary Figure 4. The average score for all the groups at both timepoints ranges from 1–2, suggesting that the bone-implant interface is mainly composed of an unorganized fibrous tissue. Only a significant difference between timepoints is observed in the Gel+MSC samples due to an improvement in the tissue response on the left side of the implants.

Figure 8 shows the combined scores for the thickness and quality of the fibrous capsule surrounding the periosteal and dural sides of the implant (as shown in the diagram in Supplementary Figure 1). The breakdown of the scores for the periosteal and dural sides of the implant can be seen in Supplementary Figure 5. Representative high magnification

images of the fibrous capsule and the respective scores for thickness and quality are shown in Supplementary Figure 6. Across all groups, no significant differences are observed between the 4 and 12 week timepoints under both scoring systems. Based on the average thickness score of ~2, the capsule was about 10–30 layers thick, but fibrous-like and well-organized, as suggested by an average quality score of ~3.

The average histological scores for hydrogel fragmentation due to tissue infiltration are shown in Figure 9. The sections were scored according to the inlaid 0–4 scoring guide in Figure 9, and representative sections are shown with respective scores. All samples demonstrated some degree of fragmentation, as seen by the average score of ~2, but only the GMP-containing hydrogels (Gel+GMP and Gel+GMP+MSC) showed significant differences from the 4 to 12 week timepoints. Additionally, only the Gel+GMP+MSC hydrogels with both GMPs and MSCs demonstrated significantly greater fragmentation from the Gel+MSC group at the 12 week timepoint.

4. Discussion

The objective of this study was to evaluate the osteogenic potential and regenerative capacity of an injectable dual-gelling hydrogel system for MSC delivery. We hypothesized that the hydrophobicity of the hydrogels and presence of natural material as controlled through TGM wt% and GMP loading, respectively, would modulate encapsulated cell viability, osteogenic differentiation, and hydrogel mineralization *in vitro*. Additionally, the composite hydrogel constructs with both GMPs and MSCs were hypothesized to enhance bone regeneration in a rat cranial defect compared to hydrogels with either GMPs or MSCs alone.

Stable hydrogels for the encapsulation of primary rat MSCs were successfully fabricated through the dual thermal and chemical gelation of the TGM and PAMAM. For the *in vitro* study, 10 and 20 wt% hydrogels with and without GMPs were examined. GMPs and cells were shown to not adversely influence hydrogel gelation, and Live/Dead and DNA Picogreen assays demonstrated that viable MSCs could be encapsulated homogenously within hydrogels for up to 28 days. Although a decline in cell viability was observed in the non-GMP-containing hydrogels, as commonly seen in the literature pertaining to synthetic hydrogels [19–22], the incorporation of GMPs improved cell viability at the later timepoints. This observation agrees with the literature in which the inclusion of a natural binding site to allow for cell attachment can improve cell survival [23]. The effect of gelatin incorporation was also observed in the production of ALP, an early osteogenic marker. ALP activity was enhanced and peaked at the 21 d timepoint in the non-GMP-containing hydrogels, which correlated well with the established profile of MSCs undergoing osteogenesis *in vitro* [13, 19]. However, ALP activity for the GMP-containing hydrogels was sustained over time, suggesting that the state of cellular attachment was directing MSC behavior [24, 25]. Indeed, previous work has established that the cellular interaction specifically with collagenous-based matrix components promotes osteogenic differentiation and cell survival compared to adsorption of other attachment proteins such as vitronectin on synthetic scaffolds [26, 27]. In another study, seeding MSCs directly onto GMPs was found to more effectively produce aggregates capable of osteogenesis due to increased cell-cell and cell-ECM interaction [28].

Hydrogel mineralization of cellular samples and acellular controls was assessed using a calcium biochemical assay. As seen previously, hydrogels demonstrated a hydrophobicity-dependent mineralization over time [3], with 20 wt% hydrogels showing significantly greater calcium content compared to 10 wt% hydrogels with and without cells. However, GMP incorporation was also found to be a significant factor, with GMP-containing hydrogels demonstrating significantly greater calcium content than their non-GMP-containing counterparts. Additionally, when MSCs and GMPs were jointly encapsulated, a significant difference from the acellular controls was observed at the 28 day timepoint. A possible explanation for this effect is that gelatin comprises denatured collagen, which is the primary ECM component of mineralized matrix, and assists in mineral nucleation [29, 30]. This mechanism has been mimicked in gelatin nanoparticles to nucleate hydroxyapatite crystals [31], and thus, provides further evidence by which hydrogel mineralization can be promoted without initially using inorganic materials, and highlights another function for GMPs in scaffolds beyond controlled release carriers and porogens.

Two concerns associated with the in vitro evaluation include the use of particular media supplements and the short culture duration, which may overstate the osteogenic potential of the hydrogel system. Thus a longer *in vivo* study was performed to investigate the actual performance of the hydrogels for bone regeneration. For the *in vivo* evaluation, we chose to further examine the 20 wt% hydrogel formulation based on its ability to maintain long-term cell viability and enhance hydrogel mineralization. Three groups were examined: hydrogels with GMPs only (Gel+GMP), hydrogels with MSCs only (Gel+MSC), and hydrogels with GMPs and MSCs (Gel+GMP+MSC). Although no significant differences were observed between groups at the 4-week timepoint, microCT scoring of bony bridging and bone volume demonstrate that there was some degree of union and bone formation in all the groups, which is a departure from previously published results with similar acellular, non-composite hydrogels in this model [3]. Similarly, no significant differences in the microCT data were seen at 12 weeks, but the hydrogels with GMPs only (Gel+GMP) showed significant differences between the 4 and 12 week timepoints. While this observation could be construed as a minimal effect of the MSCs, another interpretation may be that the incorporation and subsequent degradation of the GMPs creates pores that can facilitate tissue infiltration and ingrowth, leading to improved bony bridging and volume as seen with other porous scaffolds [32, 33] and in contrast to the limited regenerative performance previously observed with slower degrading non-GMP-containing hydrogels [3]. Despite this, significant bone fill was not observed with microCT, which may be attributed to the lack of extensive porosity and sufficient mechanical properties to promote tissue ingrowth. Further work and use of other techniques such as x-ray diffraction in addition to microCT may provide insight into the type of bone tissue formed and strategies to enhance it.

The joint effect of the MSCs and GMPs is more clearly observed when examining the histology for tissue response and integration. The majority of the samples at the 4 and 12 week timepoints presented a favorable tissue response through a thin organized fibrous capsule around the implant and at the bone-implant interface, an established response with implantation of biomaterials [34]. However, bony bridging across defect and mineralization within the different hydrogel groups was also observed, which directly contacted the

surrounding hydrogel and is typically uncharacteristic of synthetic hydrogels in this model [35, 36]. Additionally, the presence of osteoid within the center of the hydrogels, especially those containing GMPs, demonstrated that the hydrogels were capable of fragmentation leading to tissue infiltration and direct bone-implant contact. These results suggest that the dual incorporation of MSCs and GMPs can facilitate the osteoconductivity and osteoinductivity of synthetic scaffolds for enhanced bone formation and scaffold integration. Previous studies required the incorporation of mineral content or osteogenic growth factors in order to induce bone tissue infiltration in the rat cranial defect, even when GMPs were loaded as a delivery vehicle [16, 32, 35, 36]. In contrast, simple incorporation of GMPs and MSCs together in the bulk matrix led to improvements in bone formation and quality *in vivo*, leading to performances similar to that of NiPAAm copolymer macromers containing phosphate for specific interaction with alkaline phosphatase [13]. MSCs have been shown to have a multitude of paracrine effects, including secretion of factors to recruit host cells, which could positively alter the endogenous regenerative process [5]. However, the ability to achieve hydrogel fragmentation *in vivo* via GMP degradation greatly affected the underlying tissue response.

5. Conclusion

In this study, the osteogenic potential *in vitro* and regenerative capacity *in vivo* of an injectable, dual-gelling hydrogel system for MSC delivery was investigated. Hydrogels successfully and homogenously encapsulated MSCs without detriment to cell viability or hydrogel gelation, and maintained cell survival over 28 days in conjunction with incorporated GMPs. Cell-laden composite hydrogels modulated ALP activity in a GMP loading-dependent manner and significantly promoted hydrogel mineralization *in vitro. In vivo* evaluation in a rat critical size cranial defect demonstrated the ability of the cell-laden composite hydrogels to enable bony bridging across the defect and mineralization throughout the hydrogel volume and in direct contact with the surrounding hydrogel. Histological analysis showed a favorable tissue response and significant tissue infiltration resulting from *in vivo* fragmentation of the hydrogels, especially those containing GMPs. The results of this study suggest that the incorporation of natural material porogens can be successfully employed to promote cell viability and hard tissue formation in hydrogel environments. Thus, these injectable, dual-gelling hydrogels hold great promise as regenerative substrates for stem cell delivery in craniofacial tissue engineering applications.

Supplementary Material

Refer to Web version on PubMed Central for supplementary material.

Acknowledgments

Abbreviations

3D	Three dimensional
AA	Acrylic acid
AIBN	Azobisisobutyronitrile
ALP	Alkaline phosphatase
COM	Complete osteogenic media
DBA	Dimethyl-γ-butyrolactone acrylate
ECM	Extracellular matrix
FBS	Fetal bovine serum
GMA	Glycidyl methacrylate
GMP	Gelatin microparticle
^{1}H NMR	Proton Nuclear Magnetic Spectroscopy
HPLC	High Performance Liquid Chromatography
MBA	Methylene Bisacrylamide
MicroCT	Microcomputed tomography
M_n	Number average molecular weight
M_w	Weight average molecular weight
MSC	Mesenchymal stem cell
NiPAAm	*N*-isopropylacrylamide
PiP	Piperazine
PAMAM	Polyamidoamine
PBS	Phosphate buffered saline
PDI	Polydispersity index
TGM	Thermogelling macromer
VOI	Volume of interest

References

1. Kretlow JD, Young S, Klouda L, Wong M, Mikos AG. Injectable biomaterials for regenerating complex craniofacial tissues. Adv Mater. 2009; 21:3368–93.10.1002/adma.200802009 [PubMed: 19750143]

2. Vo TN, Kasper FK, Mikos AG. Strategies for controlled delivery of growth factors and cells for bone regeneration. Adv Drug Deliv Rev. 2012; 64:1292–309.10.1016/j.addr.2012.01.016 [PubMed: 22342771]

3. Vo TN, Ekenseair AK, Spicer PP, Watson BM, Tzouanas SN, Roh TT, Mikos AG. In vitro and in vivo evaluation of self-mineralization and biocompatibility of injectable, dual-gelling hydrogels for bone tissue engineering. J Control Release. 2014; 205:25–34.10.1016/j.jconrel.2014.11.028 [PubMed: 25483428]

4. Vo TN, Ekenseair AK, Kasper FK, Mikos AG. Synthesis, physicochemical characterization, and cytocompatibility of bioresorbable, dual-gelling injectable hydrogels. Biomacromolecules. 2014; 15:132–42.10.1021/Bm401413c [PubMed: 24320599]

5. Caplan AI, Correa D. The MSC: An injury drugstore. Cell Stem Cell. 2011; 9:11–5.10.1016/j.stem. 2011.06.008 [PubMed: 21726829]

6. Kim J, Yaszemski MJ, Lu L. Three-dimensional porous biodegradable polymeric scaffolds fabricated with biodegradable hydrogel porogens. Tissue Eng Part C Methods. 2009; 15:583–94.10.1089/ten.TEC.2008.0642 [PubMed: 19216632]

7. Ekenseair AK, Boere KW, Tzouanas SN, Vo TN, Kasper FK, Mikos AG. Synthesis and characterization of thermally and chemically gelling injectable hydrogels for tissue engineering. Biomacromolecules. 2012; 13:1908–15.10.1021/bm300429e [PubMed: 22554407]

8. Holland TA, Tabata Y, Mikos AG. Dual growth factor delivery from degradable oligo(poly(ethylene glycol) fumarate) hydrogel scaffolds for cartilage tissue engineering. J Control Release. 2005; 101:111–25.10.1016/j.jconrel.2004.07.004 [PubMed: 15588898]

9. Shin H, Temenoff JS, Mikos AG. In vitro cytotoxicity of unsaturated oligo[poly(ethylene glycol) fumarate] macromers and their cross-linked hydrogels. Biomacromolecules. 2003; 4:552–60.10.1021/Bm020121m [PubMed: 12741769]

10. Klouda L, Perkins KR, Watson BM, Hacker MC, Bryant SJ, Raphael RM, Kasper FK, Mikos AG. Thermoresponsive, in situ cross-linkable hydrogels based on N-isopropylacrylamide: Fabrication, characterization and mesenchymal stem cell encapsulation. Acta Biomater. 2011; 7:1460–7.10.1016/j.actbio.2010.12.027 [PubMed: 21187170]

11. Maniatopoulos C, Sodek J, Melcher AH. Bone formation in vitro by stromal cells obtained from bone marrow of young adult rats. Cell Tissue Res. 1988; 254:317–30.10.1007/BF00225804 [PubMed: 3197089]

12. Thibault RA, Scott Baggett L, Mikos AG, Kasper FK. Osteogenic differentiation of mesenchymal stem cells on pregenerated extracellular matrix scaffolds in the absence of osteogenic cell culture supplements. Tissue Eng Part A. 2010; 16:431–40.10.1089/ten.TEA.2009.0583 [PubMed: 19863274]

13. Watson BM, Vo TN, Tatara AM, Shah SR, Scott DW, Engel PS, Mikos AG. Biodegradable, phosphate-containing, dual-gelling macromers for cellular delivery in bone tissue engineering. Biomaterials. 2015; 67:286–96.10.1016/j.biomaterials.2015.07.016 [PubMed: 26232878]

14. Spicer PP, Kretlow JD, Young S, Jansen JA, Kasper FK, Mikos AG. Evaluation of bone regeneration using the rat critical size calvarial defect. Nature Protocols. 2012; 7:1918–29.10.1038/nprot.2012.113 [PubMed: 23018195]

15. Henslee AM, Spicer PP, Yoon DM, Nair MB, Meretoja VV, Witherel KE, Jansen JA, Mikos AG, Kasper FK. Biodegradable composite scaffolds incorporating an intramedullary rod and delivering bone morphogenetic protein-2 for stabilization and bone regeneration in segmental long bone defects. Acta Biomater. 7:3627–37.10.1016/j.actbio.2011.06.043 [PubMed: 21757034]

16. Patel ZS, Young S, Tabata Y, Jansen JA, Wong MEK, Mikos AG. Dual delivery of an angiogenic and an osteogenic growth factor for bone regeneration in a critical size defect model. Bone. 2008; 43:931–40.10.1016/j.bone.2008.06.019 [PubMed: 18675385]

17. Jansen JA, Dhert WJ, van der Waerden JP, von Recum AF. Semi-quantitative and qualitative histologic analysis method for the evaluation of implant biocompatibility. J Invest Surg. 1994; 7:123–34.10.3109/08941939409015356 [PubMed: 8049175]

18. Mistry AS, Pham QP, Schouten C, Yeh T, Christenson EM, Mikos AG, Jansen JA. In vivo bone biocompatibility and degradation of porous fumarate-based polymer/alumoxane nanocomposites for bone tissue engineering. J Biomed Mater Res A. 2010; 92:451–62.10.1002/jbm.a.32371 [PubMed: 19191316]

19. Temenoff JS, Park H, Jabbari E, Sheffield TL, LeBaron RG, Ambrose CG, Mikos AG. In vitro osteogenic differentiation of marrow stromal cells encapsulated in biodegradable hydrogels. J Biomed Mater Res A. 2004; 70:235–44.10.1002/jbm.a.30064 [PubMed: 15227668]

20. Park H, Temenoff JS, Tabata Y, Caplan AI, Mikos AG. Injectable biodegradable hydrogel composites for rabbit marrow mesenchymal stem cell and growth factor delivery for cartilage

tissue engineering. Biomaterials. 2007; 28:3217–27.10.1016/j.biomaterials.2007.03.030 [PubMed: 17445882]

21. Nuttelman CR, Tripodi MC, Anseth KS. Synthetic hydrogel niches that promote hMSC viability. Matrix Biol. 2005; 24:208–18.10.1016/j.matbio.2005.03.004 [PubMed: 15896949]

22. Chatterjee K, Lin-Gibson S, Wallace WE, Parekh SH, Lee YJ, Cicerone MT, Young MF, Simon CG Jr. The effect of 3D hydrogel scaffold modulus on osteoblast differentiation and mineralization revealed by combinatorial screening. Biomaterials. 2010; 31:5051–62.10.1016/j.biomaterials. 2010.03.024 [PubMed: 20378163]

23. Shin H, Zygourakis K, Farach-Carson MC, Yaszemski MJ, Mikos AG. Attachment, proliferation, and migration of marrow stromal osteoblasts cultured on biomimetic hydrogels modified with an osteopontin-derived peptide. Biomaterials. 2004; 25:895–906.10.1016/S0142-9612(03)00602-1 [PubMed: 14609678]

24. Mathieu PS, Loboa EG. Cytoskeletal and focal adhesion influences on mesenchymal stem cell shape, mechanical properties, and differentiation down osteogenic, adipogenic, and chondrogenic pathways. Tissue Eng Part B Rev. 2012; 18:436–44.10.1089/ten.TEB.2012.0014 [PubMed: 22741572]

25. Benoit DS, Schwartz MP, Durney AR, Anseth KS. Small functional groups for controlled differentiation of hydrogel-encapsulated human mesenchymal stem cells. Nat Mater. 2008; 7:816–23.10.1038/nmat2269 [PubMed: 18724374]

26. Chastain SR, Kundu AK, Dhar S, Calvert JW, Putnam AJ. Adhesion of mesenchymal stem cells to polymer scaffolds occurs via distinct ECM ligands and controls their osteogenic differentiation. J Biomed Mater Res A. 2006; 78:73–85.10.1002/jbm.a.30686 [PubMed: 16602124]

27. Marom R, Shur I, Solomon R, Benayahu D. Characterization of adhesion and differentiation markers of osteogenic marrow stromal cells. J Cell Physiol. 2005; 202:41–8.10.1002/jcp.20109 [PubMed: 15389528]

28. Hayashi K, Tabata Y. Preparation of stem cell aggregates with gelatin microspheres to enhance biological functions. Acta Biomater. 2011; 7:2797–803.10.1016/j.actbio.2011.04.013 [PubMed: 21549223]

29. Wang Y, Azais T, Robin M, Vallee A, Catania C, Legriel P, Pehau-Arnaudet G, Babonneau F, Giraud-Guille MM, Nassif N. The predominant role of collagen in the nucleation, growth, structure and orientation of bone apatite. Nat Mater. 2012; 11:724–33.10.1038/nmat3362 [PubMed: 22751179]

30. Nudelman F, Pieterse K, George A, Bomans PH, Friedrich H, Brylka LJ, Hilbers PA, de With G, Sommerdijk NA. The role of collagen in bone apatite formation in the presence of hydroxyapatite nucleation inhibitors. Nat Mater. 2010; 9:1004–9.10.1038/nmat2875 [PubMed: 20972429]

31. Ethirajan A, Ziener U, Chuvilin A, Kaiser U, Colfen H, Landfester K. Biomimetic hydroxyapatite crystallization in gelatin nanoparticles synthesized using a miniemulsion process. Adv Func Mater. 2008; 18:2221–7.10.1002/adfm.200800048

32. Ruhe PQ, Hedberg-Dirk EL, Padron NT, Spauwen PHM, Jansen JA, Mikos AG. Porous poly(dl-lactic-co-glycolic acid)/calcium phosphate cement composite for reconstruction of bone defects. Tissue Eng. 2006; 12:789–800.10.1089/ten.2006.12.789 [PubMed: 16674292]

33. Burdick JA, Frankel D, Dernell WS, Anseth KS. An initial investigation of photocurable three-dimensional lactic acid based scaffolds in a critical-sized cranial defect. Biomaterials. 2003; 24:1613–20.10.1016/S0142-9612(02)00538-0 [PubMed: 12559821]

34. Anderson JM, Rodriguez A, Chang DT. Foreign body reaction to biomaterials. Semin Immunol. 2008; 20:86–100.10.1016/j.smim.2007.11.004 [PubMed: 18162407]

35. Young S, Patel ZS, Kretlow JD, Murphy MB, Mountziaris PM, Baggett LS, Ueda H, Tabata Y, Jansen JA, Wong M, Mikos AG. Dose effect of dual delivery of vascular endothelial growth factor and bone morphogenetic protein-2 on bone regeneration in a rat critical-size defect model. Tissue Eng Part A. 2009; 15:2347–62.10.1089/ten.tea.2008.0510 [PubMed: 19249918]

36. Kretlow JD, Spicer PP, Jansen JA, Vacanti CA, Kasper FK, Mikos AG. Uncultured marrow mononuclear cells delivered within fibrin glue hydrogels to porous scaffolds enhance bone regeneration within critical-sized rat cranial defects. Tissue Eng Part A. 2010; 16:3555–68.10.1089/ten.TEA.2010.0471 [PubMed: 20715884]
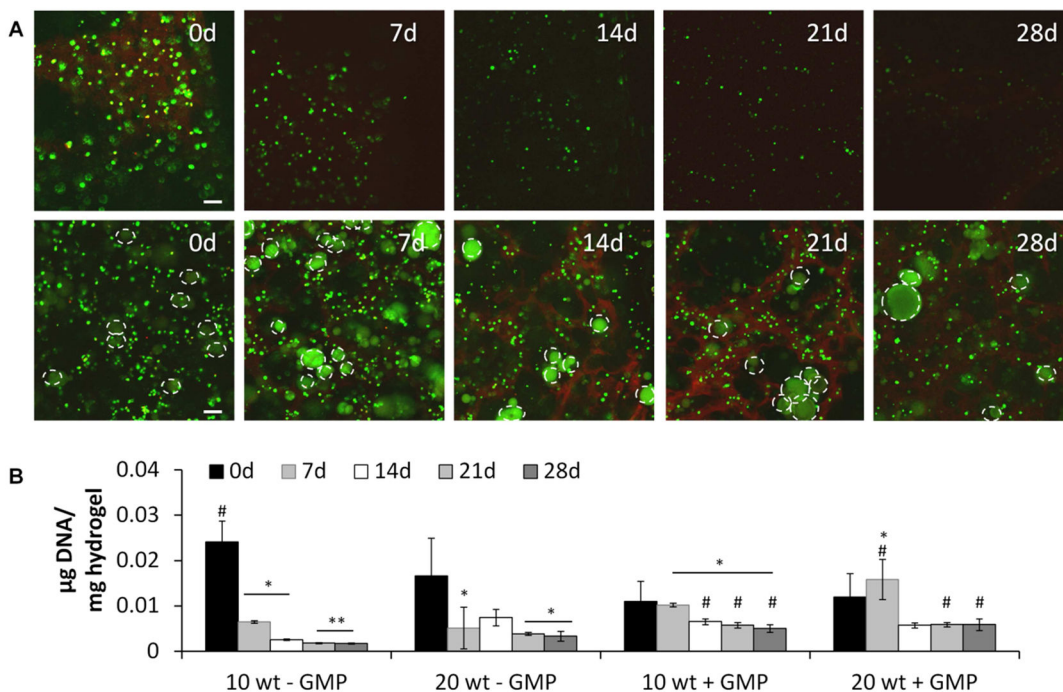
Figure 1.
A) Representative Live/Dead confocal microscopy images of 10 wt% groups with 15 million cells/mL hydrogel with (bottom row) and without (top row) gelatin microparticle (GMP) incorporation and B) DNA content of cell-laden hydrogels after culture in complete osteogenic medium for 0, 7, 14, 21, and 28 days. In confocal images, live cells (small diameter) and autofluorescing GMPs (large diameter, indicated by white dashed outline) stain green, and dead cells stain red. Scale bar in confocal images indicates 100 μm. (*), (**), and (#) indicate significant difference from 0 day timepoint, 0 and 7 day timepoints, or from non-GMP containing group at the same timepoint, respectively ($p<0.05$). Error bars indicate standard deviation (n=3–4). Confocal images demonstrating 20 wt% hydrogels performing similarly can be seen in Supplementary Figure 3.
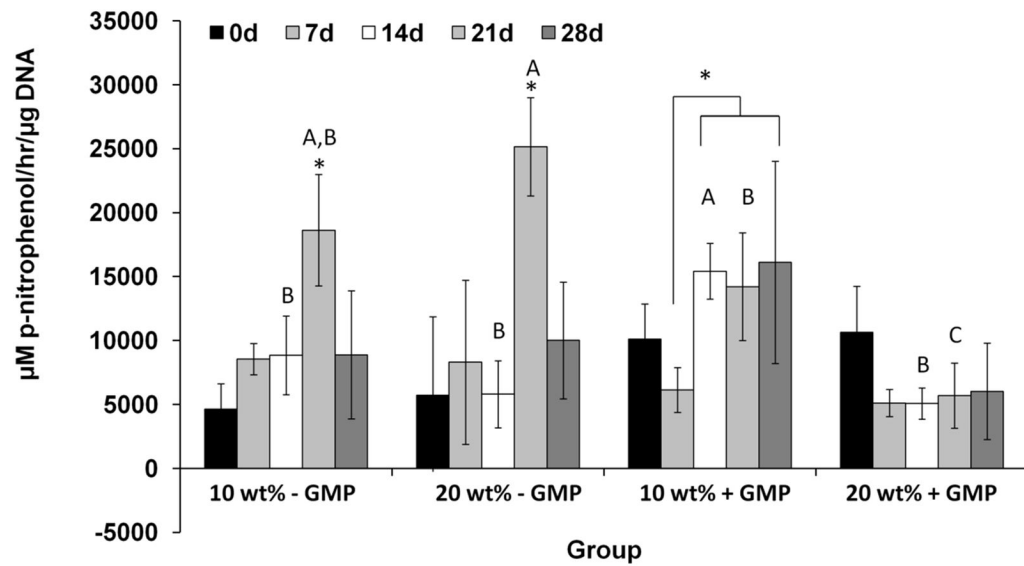
Figure 2.
Alkaline phosphatase activity of 10 and 20 wt% cell-laden hydrogels with and without gelatin microparticles (GMPs) after culture in complete osteogenic medium after 0, 7, 14, 21, and 28 days. (*) indicates significant difference across timepoints in the same group (p<0.05). Letters A–C indicate differences across groups at the same timepoint. Bars with different letters indicate significant difference (p<0.05). Unmarked bars show no significant difference. Error bars indicate standard deviation (n=3–4).
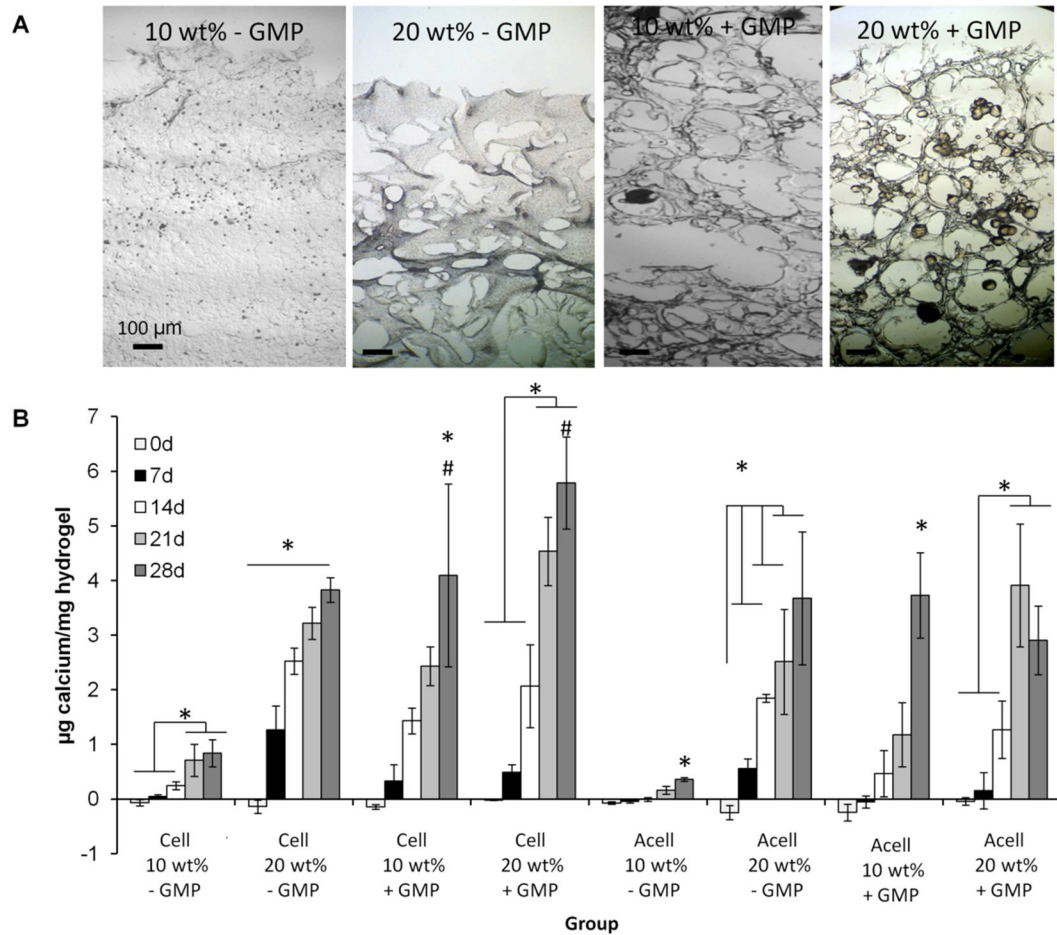
Figure 3.
A) Representative von Kossa histological sections at 28 days and B) calcium content of cell-laden hydrogels (Cell) and acellular controls (Acell) after culture in complete osteogenic medium for 0, 7, 14, 21, and 28 days. Von Kossa stains phosphate deposits black-brown. (*) and (#) indicate significant differences between timepoints in the same group or from the corresponding acellular control at the same timepoint, respectively (p<0.05). Error bars indicate standard deviation (n=3–4).
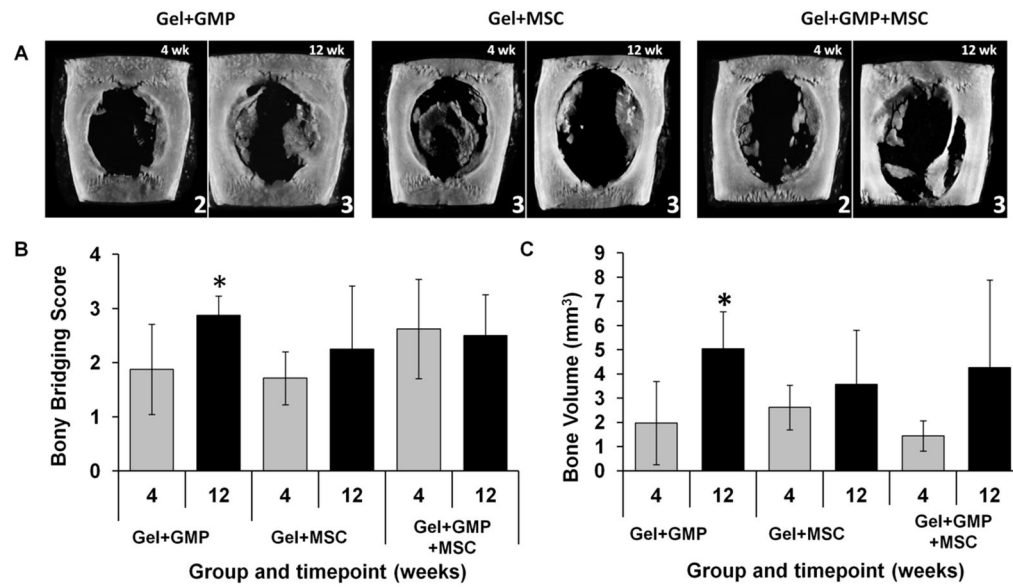
Figure 4.
A) Representative maximum intensity projections with the respective scores and B) bony bridging score and bone volume as determined by microcomputed tomography (microCT). Bony bridging was scored using the guide in Supplementary Table 1. Bone volume was quantified within an 8 mm x 2 mm volume of interest. (*) indicates significant difference between the 4 and 12 week timepoints ($p < 0.05$). Error bars indicate standard deviation (n=7–8).
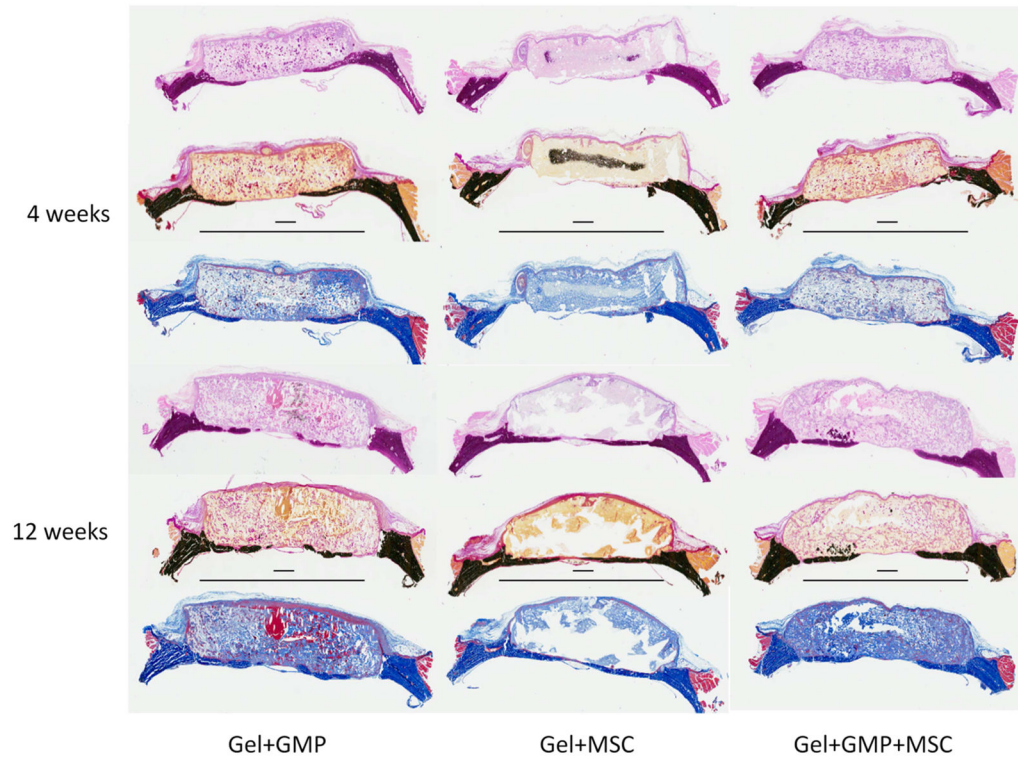
Figure 5.
Representative histological cross sections of hematoxylin & eosin (H&E) (top), von Kossa (middle), and Goldner's trichrome (bottom) stains of hydrogels with GMPs only, MSCs only, or both GMPs and MSCs at the 4 and 12 week timepoints. Scale bars below the von Kossa stain indicate 1 mm and 8 mm, respectively.
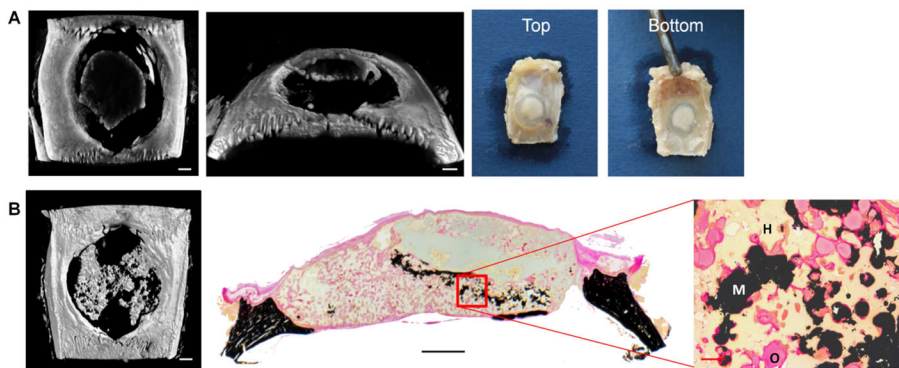
Figure 6.
Visualization and distribution of hydrogel mineralization using different techniques. A) Microcomputed tomography (microCT) generated image and optical picture of a Gel+MSC specimen at 4 weeks demonstrating mineralization at the top of the hydrogel, which can be observed grossly as opaque white mass on the translucent hydrogel. B) MicroCT generated maximum intensity projection and von Kossa stain of a Gel+GMP+MSC sample at 12 weeks, demonstrating mineral deposits through the hydrogel volume and in direct contact with the surrounding hydrogel. Scale bars in microCT images indicate 1 mm. Scale bars in histology cross section and high magnification image indicate 1 mm and 100 μm, respectively. H, M, and O in the histology image mean hydrogel, mineral, and osteoid, respectively.
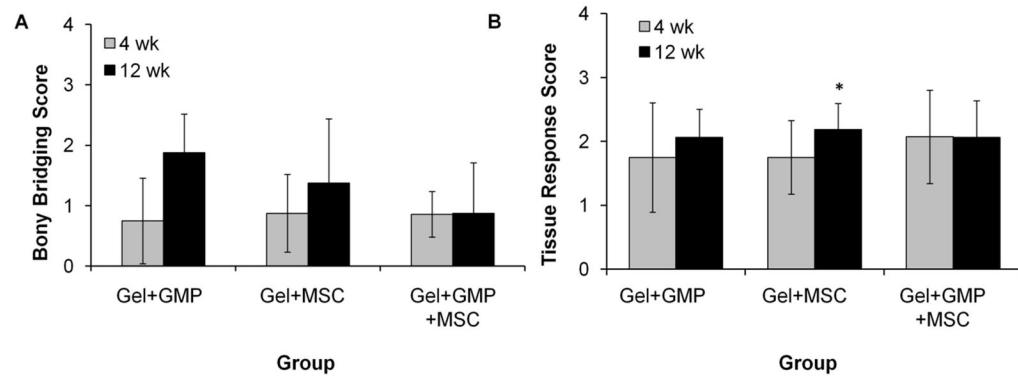
Figure 7.
Histological scoring of A) bony bridging and B) combined tissue response at the left (L) and right (R) bone-implant (total) interface of hydrogels with GMPs only (Gel+GMP), MSCs only (Gel+MSC) or both GMPs and MSCs (Gel+GMP+MSC). (*) indicates significant difference between the 4 and 12 week timepoints (p<0.05). Error bars indicate standard deviation (n=7–8). Average scores for the L and R interfaces can be found in Supplementary Figure 4.
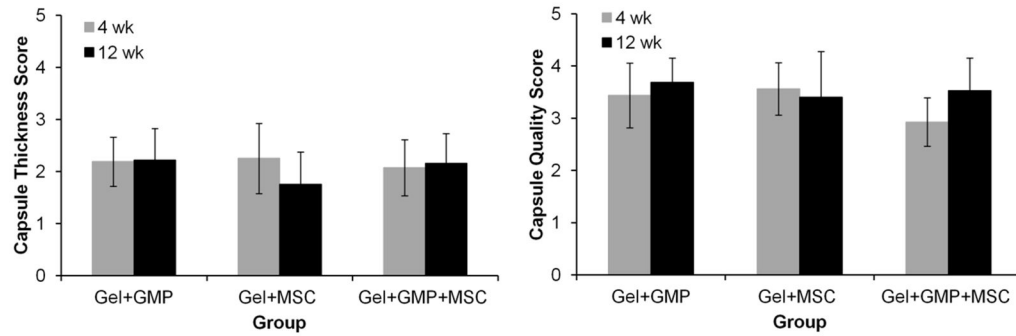
Figure 8.
Combined histological scores of fibrous capsule thickness and quality at two locations on the periosteal (top) and dural (bottom) sides of the hydrogel. Gel+GMP, Gel+MSC, and Gel +GMP+MSC correspond to hydrogels with GMPs only, hydrogels with MSCs only, or hydrogels with both GMPs and MSCs. Error bars indicate standard deviation (n=7–8). Breakdown of scores at the top and bottom of the hydrogels can be found in Supplementary Figure 5.
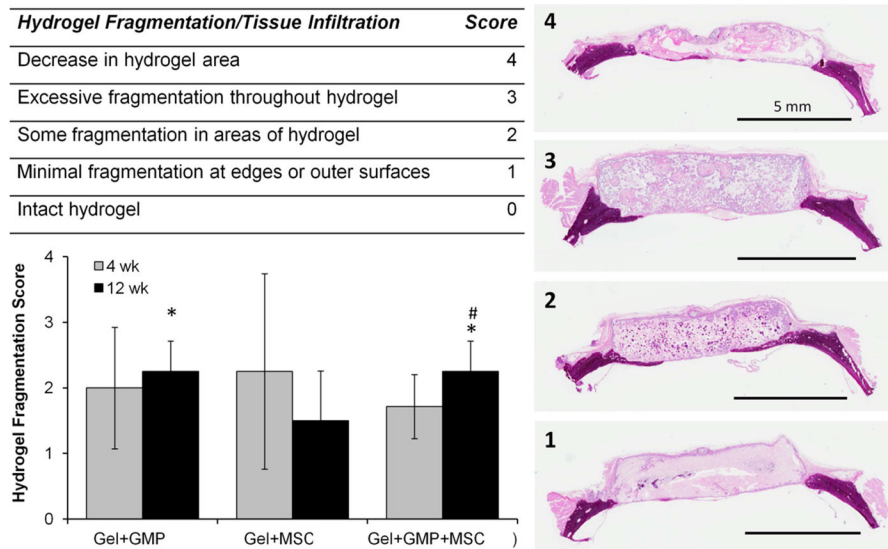
Hydrogel Fragmentation/Tissue Infiltration	Score
Decrease in hydrogel area	4
Excessive fragmentation throughout hydrogel	3
Some fragmentation in areas of hydrogel	2
Minimal fragmentation at edges or outer surfaces	1
Intact hydrogel	0

Figure 9.

Histological scoring of hydrogel fragmentation correlating with tissue infiltration on a 0–4 scale. Representative histological sections and their respective scores are shown on the right. Gel+GMP, Gel+MSC, and Gel+GMP+MSC correspond to hydrogels with gelatin GMPs only, hydrogels with MSCs only, or hydrogels with both GMPs and MSCs. (*) and (#) indicate significant differences between the 4 and 12 week timepoints or from the Gel+MSC group at the same timepoint, respectively ($p < 0.05$). Error bars indicate standard deviation (n=7–8).

Table 1

Study design evaluating the effect of TGM wt% and GMP loading on *in vitro* MSC encapsulation

Group	TGM wt% (mg TGM/100 µL PBS)	GMP Loading (mg GMP/100 mg hydrogel)	Encapsulation Density (cells/mL hydrogel)
1	10	0	1.5×10^7
2	20	0	1.5×10^7
3	10	20	1.5×10^7
4	20	20	1.5×10^7

Table 2

Study design evaluating the effect of GMP and/or MSC encapsulation on *in vivo* bone regeneration

Group	TGM wt% (mg TGM/100 μl PBS)	GMP loading (mg GMP/100 mg hydrogel)	Encapsulation Density (cells/mL hydrogel)
Gel+GMP	20	20	0
Gel+MSC	20	0	1.5×10^7
Gel+GMP+MSC	20	20	1.5×10^7